

# 3D Gaussian Splatting with Self-Constrained Priors for High Fidelity Surface Reconstruction

## Supplementary Material

### 1. Implementation Details

We follow 3DGS [2] in experimental setting. We adopt the same optimization schedule to train 30000 iterations with Adam optimizer and start from randomly initialized Gaussian attributes. The TSDF grid  $f^t$  is updated every 5000 iterations up to iteration 20000. The bandwidth scaling is set to 1, 0.5, 0.25 in each updated  $f^t$ , respectively. We enable  $L_{SCP}$  at 10000 iteration and use a decision threshold  $\delta^t = 0.3$  on  $f^t$  to label Gaussians for  $L_{SCP}$ . All experiments run on a single NVIDIA RTX 4090 GPU.

### 2. Optimization Details

**Rendering Losses.** During rendering optimization, we supervise the learning of 3D Gaussians using a unified image reconstruction loss  $L_{RGB}$ , which comprises three components: a MAE loss  $L_{MAE}$  that constrains pixel-level differences, a SSIM loss  $L_{SSIM}$  that preserves structural consistency, and a NCC loss  $L_{NCC}$  that enforces multi-view consistency. Together, these terms enable the model to achieve accurate color reconstruction, maintain structural fidelity, and ensure geometric consistency across views.

$$L_{RGB} = (1 - \beta)L_{MAE}(v_{gt}, v_{pred}) + \beta L_{SSIM}(v_{gt}, v_{pred}) + (1 - L_{NCC}(v_r(h_r), v_n(H_{rm}h_r))), \quad (1)$$

where  $\beta$  is the balance weight.  $v_{gt}$  and  $v_{pred}$  denote the ground-truth and rendered views, respectively.  $v_r$  and  $v_n$  represent the reference and target views.  $h_r$  is the homogeneous pixel coordinate in the reference view, and  $H_{rm}$  is the corresponding homography matrix.

**Signed Distance Inference for 3D Gaussians.** As described in Sec. 3.1, unlike previous methods that fit an implicit field from Gaussian points, we predict the signed distance for each Gaussian point  $q_i = [x_i, y_i, z_i]$  using the implicit prior  $f^t$ . We efficiently interpolate the distance using trilinear interpolation,

$$f^t(q_i) = a_0 + a_1x_i + a_2y_i + a_3z_i + a_4x_iy_i + a_5x_iz_i + a_6y_iz_i + a_7x_iy_iz_i, \quad (2)$$

where  $\{a_0, \dots, a_7\}$  are the interpolation weights of the TSDF grid vertices surrounding  $q_i$ .

### 3. More Comparisons and Results

In this subsection, we conduct additional ablation studies on the DTU dataset under the default parameter settings and

provide more visual results and comparisons on both synthetic and large-scale scene datasets.

**Effect of Opacity Constraint Threshold.** We analyze the effect of the opacity constraint threshold  $\delta^t$  on splitting 3D Gaussians into on-surface and off-surface subsets. Specifically, we add noise to surface points to evaluate the accuracy of  $f^t$  under different thresholds. We set  $\delta^t$  to 0.7, 0.5, 0.3, and 0.1, respectively. As shown in Fig. 1, a lower value of  $\delta^t$  makes Gaussians more sensitive to be classified as off-surface points, while the higher ones relaxes the threshold but decreases the supervision accuracy. We further visualize the Gaussian classification results of  $f^t$  under different settings. When  $\delta^t$  is set to 0.1, most on-surface points are incorrectly labeled as outliers. In contrast,  $f^t$  tends to label outliers as surface points as  $\delta^t$  is higher than 0.3. To balance robustness and accuracy, we set  $\delta^t$  to 0.3 by default.

**Visual Comparisons on NeRF-Synthetic.** We provide additional comparisons in Fig. 2. compared with implicit-field-based approaches (GS-Pull [4] and GS-UDF [3]), our method reconstructs more complete surfaces in open-surface scenarios. In contrast to TSDF based methods (QGS [5] and PGSR [1]), our approach leverages geometric priors to better preserve edge structures and reduce outliers and truncation artifacts on the boat hull or plate. Our method also recovers local details in scenes with complex textures. We further provide serial rendering visualization and evaluation in our video.

**Visualization on DTU.** We also present qualitative results on the DTU dataset in Fig. 3. As shown in Fig. 3, our method recovers more accurate surfaces in regions with complex geometric topology and maintains consistency across various open scenes.

**Visualization on TNT and Mip-NeRF 360.** We further validate the geometry inference and novel view rendering performance for our method on large-scale scenes (TNT and Mip-NeRF 360) in Fig. 4 and Fig. 5. As shown in Fig. 4, our method recovers accurate geometric structures in both complex indoor and outdoor environments. Moreover, we produce high-fidelity rendered views under low-texture regions and challenging lighting conditions in Fig. 5.

### 4. Optimization Terms Explanation

**Mean Absolute Error (MAE).** SSIM evaluates the perceptual similarity between two views considering contrast and structure. Given the ground-truth view  $v_{gt}$  and the predicted view  $v_{pred}$ , the MAE loss computes the average absolute

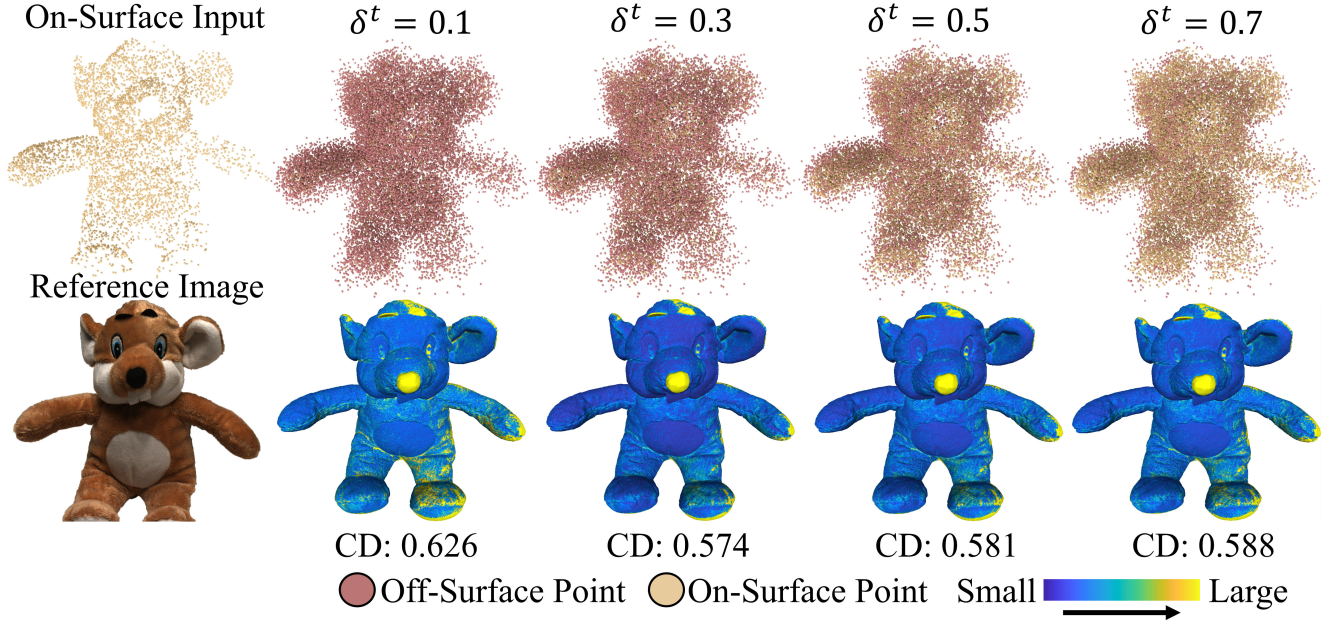


Figure 1. Effect of Opacity Constraint Threshold.

pixel-wise difference and is formulated as,

$$L_{MAE}(v_{gt}, v_{pred}) = |v_{gt} - v_{pred}|. \quad (3)$$

**Structural Similarity (SSIM).** SSIM evaluates the perceptual similarity between two views considering luminance, contrast, and structure. Given the ground-truth view  $v_{gt}$  and the predicted view  $v_{pred}$ , the SSIM is defined as,

$$L_{SSIM}(v_{gt}, v_{pred}) = \frac{(2\mu_{gt}\mu_{pred} + T_1)(2\sigma_{gt,pred} + T_2)}{(\mu_{gt}^2 + \mu_{pred}^2 + T_1)(\sigma_{gt}^2 + \sigma_{pred}^2 + T_2)}, \quad (4)$$

where  $\mu_{gt}$  and  $\mu_{pred}$  are means,  $\sigma_{gt}^2$  and  $\sigma_{pred}^2$  are the variances,  $\sigma_{gt,pred}$  is the covariance between  $v_{gt}$  and  $v_{pred}$ ,  $T_1$  and  $T_2$  are constants.

**Normalized Cross-Correlation (NCC).** NCC measures the linear correlation between two views after removing their mean intensities. Given the ground-truth view  $v_{gt}$  and the predicted view  $v_{pred}$ , the NCC is defined as,

$$L_{NCC}(v_{gt}, v_{pred}) = \frac{\sum_{i=1}^N (v_{gt}^{(i)} - \mu_{gt})(v_{pred}^{(i)} - \mu_{pred})}{\sqrt{\sum_{i=1}^N (v_{gt}^{(i)} - \mu_{gt})^2} \sqrt{\sum_{i=1}^N (v_{pred}^{(i)} - \mu_{pred})^2}}, \quad (5)$$

where  $i$  is the pixel index and  $N$  is the total number of pixels.  $\mu_{gt}$  and  $\mu_{pred}$  denote the mean intensities of all pixels in  $v_{gt}$  and  $v_{pred}$ , respectively.

## 5. Codes

We provide a demonstration code as a part of our supplementary materials. We will release the source code and data upon acceptance.

## 6. Video

We provide a video containing the visualizations on all datasets as a part of our supplementary materials.

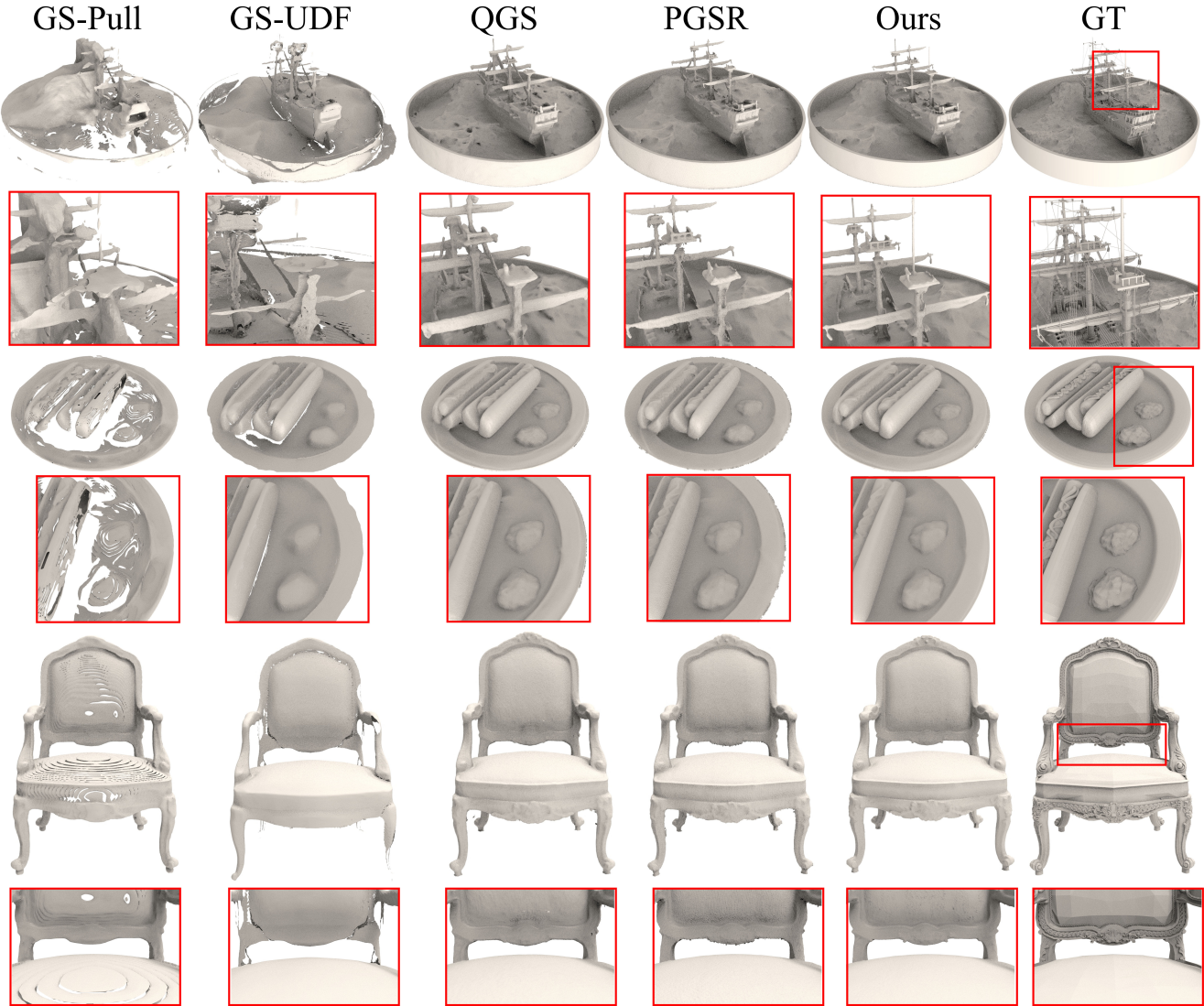


Figure 2. Visual Comparisons on NeRF-Synthetic Dataset.



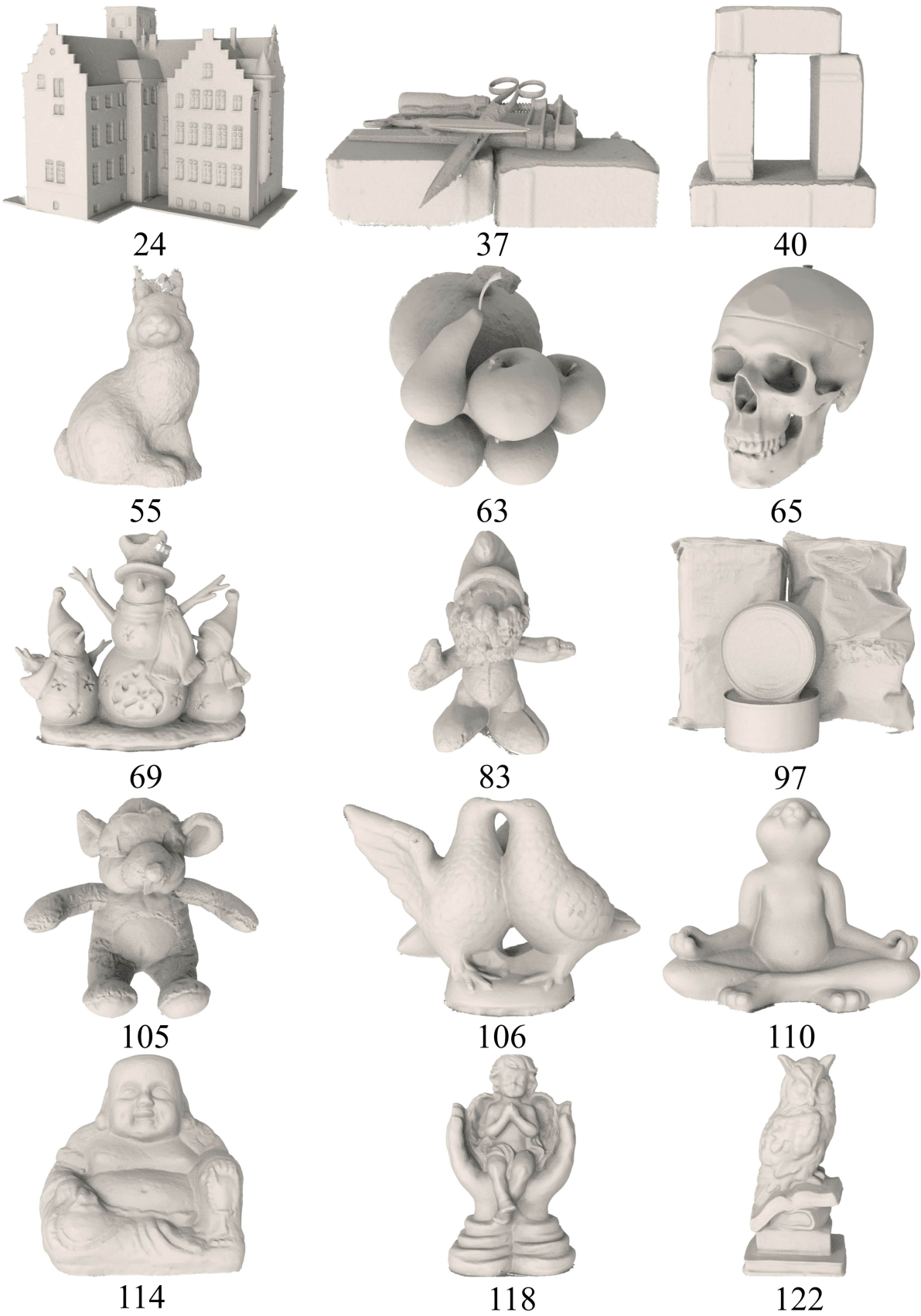


Figure 3. Visual Comparisons on DTU Dataset.





Figure 4. Surface Reconstruction Visualization on TNT and Mip-NeRF 360 Dataset.

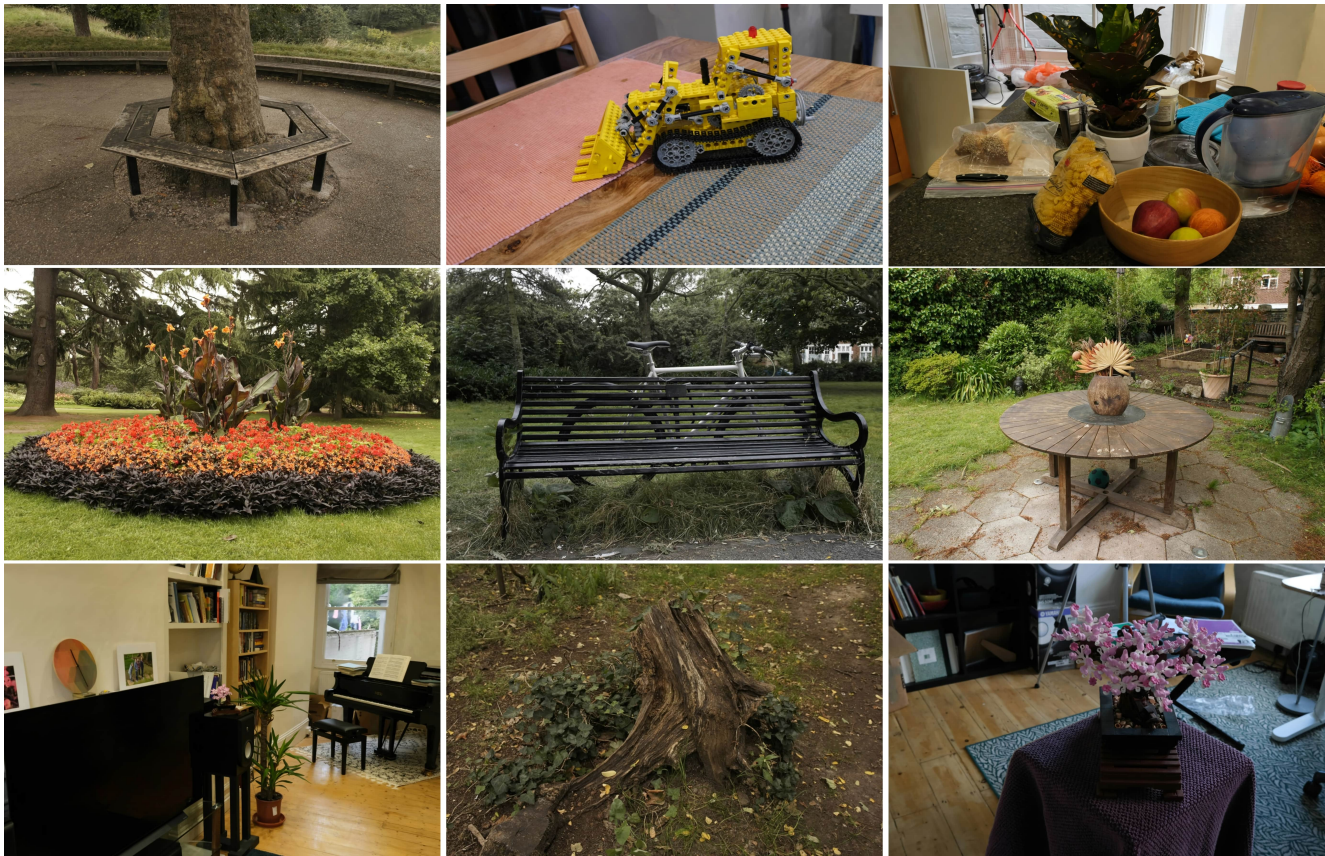


Figure 5. Rendering Visualization on Mip-NeRF 360 Dataset.

114

**References**

115

116

117

118

119

120

121

122

123

124

125

126

127

128

129

130

131

132

133

134

135

136

137

- [1] Danpeng Chen, Hai Li, Weicai Ye, Yifan Wang, Weijian Xie, Shangjin Zhai, Nan Wang, Haomin Liu, Hujun Bao, and Guofeng Zhang. PGSR: Planar-based gaussian splatting for efficient and high-fidelity surface reconstruction. *IEEE Transactions on Visualization and Computer Graphics*, 2024. 1
- [2] Bernhard Kerbl, Georgios Kopanas, Thomas Leimkühler, and George Drettakis. 3D gaussian splatting for real-time radiance field rendering. *ACM Transactions on Graphics*, 42(4):1–14, 2023. 1
- [3] Shujuan Li, Yu-Shen Liu, and Zhizhong Han. Gaussianudf: Inferring unsigned distance functions through 3d gaussian splatting. In *Proceedings of the IEEE/CVF Conference on Computer Vision and Pattern Recognition*, 2025. 1
- [4] Wenyuan Zhang, Yu-Shen Liu, and Zhizhong Han. Neural signed distance function inference through splatting 3d gaussians pulled on zero-level set. In *Advances in Neural Information Processing Systems*, 2024. 1
- [5] Ziyu Zhang, Binbin Huang, Hanqing Jiang, Liyang Zhou, Xiaojun Xiang, and Shuhan Shen. Quadratic gaussian splatting: High quality surface reconstruction with second-order geometric primitives. In *Proceedings of the IEEE/CVF International Conference on Computer Vision*, pages 28260–28270, 2025. 1